Impedance Matching for the Multilayer Medium—Toward a Design Methodology

Kai M. Hock

***Abstract*—A graphical analysis of the impedance matching problem for the multilayer dielectric and magnetic coating of metallic surfaces, for normal plane wave incidence, is presented, with a view to providing insight into design principles. Methods for visual design using Smith-chart-type graphical tools, which can complement computationally intensive optimization, are derived. The problem of estimating the required permittivity and permeability for given frequency and thickness is also discussed.**

***Index Terms*—Impedance matching, microwave, multilayer.**

I. Introduction

ELECTROMAGNETIC wave reflection and transmission by multilayer media have been extensively studied because of its wide applications. Examples include radio wave propagation through stratified layers of the atmosphere [1], microwave impedance matching in multilayer media [2]–[4], and multilayer structures for optical devices [5], [6]. This paper focuses on the problem of microwave reflection from a metal backed multilayer medium. The objective is to investigate the problem of impedance matching in this structure.

The reason for the choice of a multilayer medium in microwave applications should be highlighted. The single-layer homogeneous medium does not provide a sufficient degree of freedom for broad-band impedance matching. The only adjustable parameters, apart from thickness, are the permittivity and permeability which are difficult to adjust. In order to overcome this restriction, much work has been done to investigate the properties of different structures such as multilayer media, doubly periodic surfaces [8], and chiral materials [9]. The structures may combine more than one material. Each material alone has permittivity and permeability that usually cannot provide adequate matching if used as a single layer. By combining and shaping them, it is often hoped that electromagnetic compatibility can be achieved to a greater extent than using one material alone, and this constitutes the design problem for these structures.

This paper focuses on the problem for multilayer structures. Much of the work done in this area makes use of optimization methods [10]–[14], and a popular choice of optimization method is the genetic algorithm (GA). These "design" methods make use of optimization completely, with little or no consideration for the behavior of microwave transmission. However, the very need for optimization methods arose because of the large number of parameters involved for all the layers—permittivity, permeability, thickness, and wavelength. This means that a global search on all possible combinations is far too computationally intensive and cannot be achieved in a reasonable time even for a small number of layers. Hence, if it were possible to reduce the optimization task by enabling some amount of intuitive work, there should be great savings in computational resources.

Manuscript received February 19, 2002; revised September 19, 2002. This work was supported by the Directorate of Research and Development, Defence Science and Technology Agency, Singapore.

The author is with the Temasek Laboratories, National University of Singapore, Singapore 119260 (e-mail: tslhkm@nus.edu.sg).

Digital Object Identifier 10.1109/TMTT.2003.808664

II. A Graphical Analysis

The multilayer system studied consists of a number of homogeneous layers, each of uniform thickness, coated on a perfectly conducting metal surface. This paper follows the convention of [15], in which the layer in contact with the air is labeled 1, and the layer closest to the metal surface is labeled M-1. The corresponding thickness, permittivity, and permeability for layer m are respectively given by h_m, ε_m, and μ_m (whose real and imaginary parts are defined by $\varepsilon = \varepsilon' - i\varepsilon''$ and $\mu = \mu' - i\mu''$). Conductivity σ_m is assumed to be zero for all layers, and only normal incidence is considered, so that the incidence angle θ is zero. The equations in [15] for reflection coefficient then reduce to

$$R_0 = \frac{K_0 - Z_1}{K_0 + Z_1} \tag{1}$$

where Z_1 is given by the recursive relation

$$Z_{m-1} = K_{m-1}\left[\frac{Z_m + K_{m-1}\tanh(U_{m-1}h_{m-1})}{K_{m-1} + Z_m\tanh(U_{m-1}h_{m-1})}\right] \tag{2}$$

and where

$$K_m = \sqrt{\frac{\mu_m}{\varepsilon_m}} \text{ and } U_m = j\omega\sqrt{\mu_m\varepsilon_m} \tag{3}$$

for $m = 1$ to $M-1$, with $Z_M = 0$. (Note that the subscripts, whether m or $m-1$, are just dummy variables. In (2), $m = 2$ to $M-1$ only, and $m = 1$ is not needed, so that Z_0 does not exist. When $m = 2$ in (2), for example, $K_{m-1} = K_1$, and this is to be evaluated in (3) by setting $m = 1$ there.)

Instead of using these to vary the parameters and search for the lowest reflection amplitude by optimization methods, the idea is used to visualize the Z_m for each layer graphically, like on a Smith chart.

To illustrate the method, the hypothetical data set (reproduced in Table I) for the five-layer coating labeled HF2 in [10] is used. In Fig. 1, the result of mapping Z_m using (1) (taking Z_0 as Z_m) for each layer is shown. To understand this, consider first the

TABLE I
RELATIVE PERMITTIVITIES AND PERMEABILITIES OF THE 16 MATERIALS IN THE DATABASE

Lossless Dielectric Materials (μ_r=1+j0)		
#	ε_r	
1	10+j0	
2	50+j0	
Lossy Magnetic Materials (ε_r =15+j0)		
$\mu=\mu_r-j\mu_i$ $\quad \mu_r(f)=\frac{\mu_r(1GHz)}{f^{\alpha}}$ $\quad \mu_i(f)=\frac{\mu_i(1GHz)}{f^{\beta}}$		
#	μ_r(1GHz), α	μ_i(1GHz), β
3	5, 0.974	10, 0.961
4	3, 1.000	15, 0.957
5	7, 1.000	12, 1.000
Lossy Dielectric Materials (μ_r =1+j0)		
$\varepsilon=\varepsilon_r-j\varepsilon_i$ $\quad \varepsilon_r(f)=\frac{\varepsilon_r(1GHz)}{f^{\alpha}}$ $\quad \varepsilon_i(f)=\frac{\varepsilon_i(1GHz)}{f^{\beta}}$		
#	ε_r(1GHz), α	ε_i(1GHz), β
6	5, 0.861	8, 0.569
7	8, 0.778	10, 0.682
8	10, 0.778	6, 0.861
Relaxation-type Magnetic Materials (ε_r =15+j0)		
$\mu=\mu_r-j\mu_i$ $\quad \mu_r=\frac{\mu_{rm}f_m^2}{f^2+f_m^2}$ $\quad \mu_i=\frac{\mu_{rm}f_m f}{f^2+f_m^2}$ (f and f_m in GHz)		
#	μ_{rm}	f_m
9	35	0.8
10	35	0.5
11	30	1.0
12	18	0.5
13	20	1.5
14	30	2.5
15	30	2.0
16	25	3.5

*Reproduced from ref. [10]

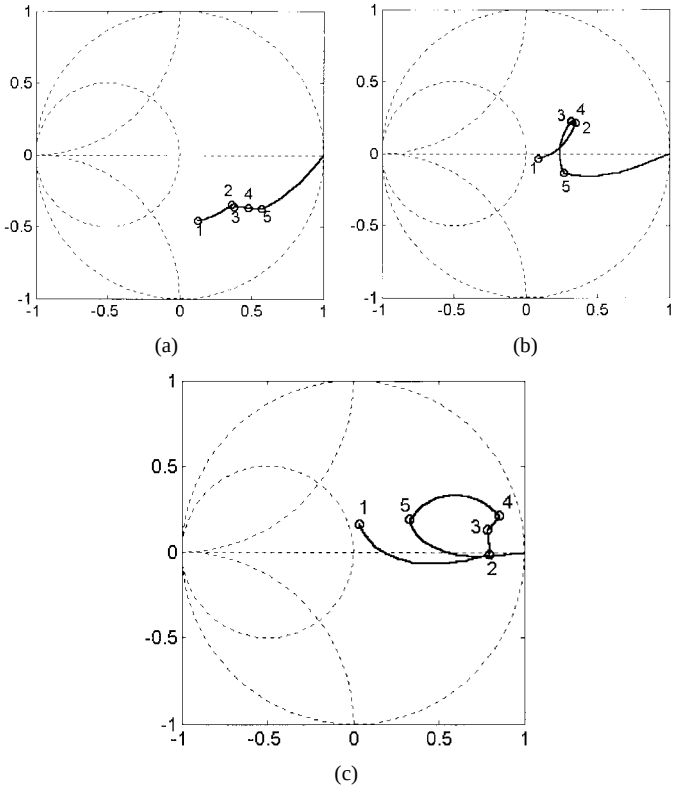

Fig. 1. Mapping of Z_m to R, based on parameters of the coating labeled HF2 in [10], at: (a) 1 GHz, (b) 3 GHz, and (c) 10 GHz. HF2 consists of layers $m = 1$ to 5, made up of materials number 16, 8, 5, 2, and 13, with thicknesses 0.537, 0.432, 0.261, 0.465, and 0.975 mm, respectively.

metal surface with no coating. Since $K_6 = 0$, the mapping in (1) gives $R_0 = 1$, which is represented by the closed circle in Fig. 1. Equation (2) is then applied recursively to give Z_5, Z_4, Z_3, Z_2 and Z_1. These are mapped to the complex R plane in Fig. 1, and labeled 5 to 1, respectively. The mapping used is based on (1), which can be written in the form $R = (1 - z)/(1 + z)$. It is carried out by repeatedly setting z to Z_m/K_0, where m is 5 to 1. The curve joining Z_m to Z_{m-1} is obtained using (2) by varying h_{m-1} from 0 to the actual thickness. For instance, the curve between points 5 and 4 is obtained from

$$Z = K_4 \left[\frac{Z_5 + K_4 \tanh(U_4 h)}{K_4 + Z_5 \tanh(U_4 h)} \right] \tag{4}$$

by varying h from 0 to h_4 and mapping Z to the R plane.

In Fig. 1, the dotted curves are the unit circles from the admittance Smith chart. We used this instead of the impedance Smith chart because of the form of (1). The impedance Smith chart results from the mapping $R = (z - 1)/(z + 1)$, whereas (1) is of the form $R = (1 - z)/(1 + z)$, which corresponds to a 180° rotation. Whichever one is plotted, it is clear that the material curves in Fig. 1 do not follow those in either form of the Smith charts. While we can still think in terms of capacitance and inductance by moving down or up on a Smith chart, a different set of charts are needed for quantitative analysis. (A similar use of the Smith chart has been discussed in [7] for the multilayer resistive sheet and in [8] for the frequency-selective surface.)

In order to have a design method, it is necessary to look for behaviors that are more universal in nature. This need, together with the idea behind the Smith chart, suggests that it may be useful to create a trajectory plot or a quiver plot from (2) for each material of the coating. A trajectory plot consists of a family of possible trajectories for each material, as illustrated in Fig. 2, such that each trajectory corresponds to the mapping of Z_{m-1} for a given Z_m in (2). On the other hand, a quiver plot consists of a collection of arrows, and each arrow is located on the complex R plane, indicating the change of R for a small increment in h, like in Fig. 3.

A trajectory in a trajectory plot may be created as follows. Select any point on the unit circle, i.e., $|R| = 1$. Substitute this into R_0 in (1) and calculate Z_1. (Do not associate Z_1 with layer 1. Just treat it as a dummy variable. Likewise for R_0.) Next, substitute Z_1 into Z_m in (2). Calculate K_m from (3) by taking ε_m and μ_m as the permittivity and permeability of the material of interest and substitute it into K_{m-1} in (2). Then, by increasing h_{m-1} from zero in small steps, calculate a series of Z_{m-1} from (2). Substitute each Z_{m-1} into Z_1 in (1), calculate R_0, and plot them on the complex plane. This gives the trajectory.

Each arrow in the quiver plot may be created as follows. Consider a point inside the unit circle. Suppose that this represents the reflectivity R_0 of a certain coating. Suppose now that an additional layer of the same material, with relative permittivity ε_r, relative permeability μ_m, and of thickness δh, is added. Using (6), which is explained in the next section, calculate

$$\delta R \approx \left. \frac{dR}{dh} \right|_{h=0} \delta h. \tag{5}$$

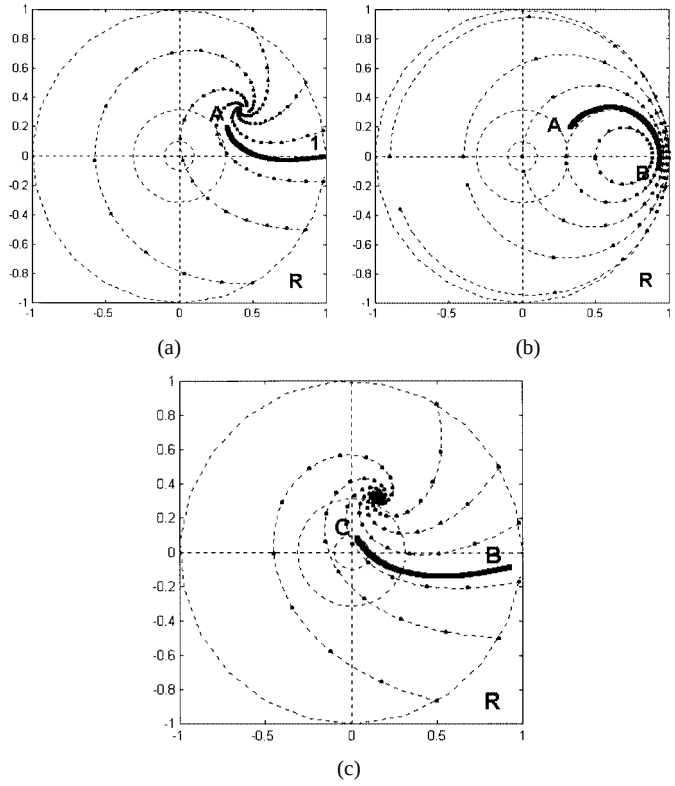

Fig. 2. Trajectory plots at 10 GHz for materials: (a) number 13, (b) number 2, and (c) number 16 of [10]. The two concentric circles at the center of each figure correspond to -20 dB (for the smaller one) and -10 dB (for the larger one) reflection.

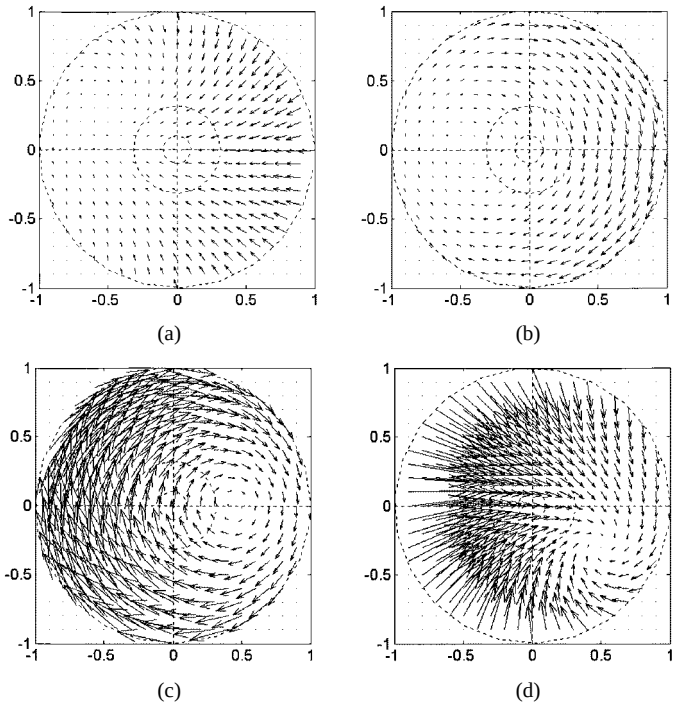

Fig. 3. Quiver plots showing the general arrow directions for four extreme cases of permittivity and permeability. Each plot shows the contributions from the material properties of a thin layer with thickness δh to the change in reflectivity. The calculation is carried out at a frequency of 3 GHz for the values of the properties indicated.

$Z' = Z/K_0$ in (6) is obtained by calculating Z_1 from R_0 in (1) and then substituting Z_1 into Z. δR is a complex number which can be represented as a vector. This gives the required arrow. This is repeated for a regular set of points, and the quiver plot is obtained.

The trajectory and quiver plots are useful not only to provide visualization of the multilayer design, but also to give insight into to the process. For instance, it is known that R must always start from 1. (For the metal surface alone without any coating, $R_0 = 1$ from (1), since $Z_1 = 0$.) We may then try to design a multilayer structure using the three materials in Fig. 2. The trajectory plot makes it possible to see at one glance the path that a curve joining the mapping of any two points, Z_{m-1} and Z_m. For instance, if material number 13 is chosen to be the layer in contact with the metal surface, the solid arrow shown in Fig. 2(a) going from $R = 1$ to point A is the only possible path, but this does not approach the neighborhood of $R = 0$. If materials 2 and 16 are available, we may then make use of their trajectory plots in Figs. 2(b) and (c), respectively, to find a suitable path. If the next layer is chosen to be material number 16, Fig. 2(c) shows that it still could not bring the path from point A anywhere closer to $R = 0$. If material number 2 is chosen, however, we could first follow a path from point A to point B. Then B can be adjusted by varying the thickness of material 2 [Fig. 2(b)] such that the addition of material number 16 as a third layer would be able to bring point B to point C, which is much closer to $R = 0$ [Fig. 2(c)]. Although it may be argued that this is only obvious from hindsight after Fig. 1 has been obtained, the possibility of practical design using the trajectory plots is nevertheless promising because of the simplicity of the procedure. For instance, the thickness of each layer is immediately obvious because the length of each arrow is easily estimated, e.g., the distance between adjacent dots on each trajectory in Fig. 2 is 0.1 mm.

The above approach is in fact a visualization of the formalism used for optimization in [2]. There, the sum of the length of the trajectories and distance between the final end point of the trajectories and $R = 0$ is used directly as an optimization cost function. What is new here is the suggestion of creating the trajectory plots and using them as a design tool before launching into full-scale optimization.

The calculations and visualization in Fig. 1 have been repeated for all of the 13 optimized coatings given in [10]. It is found that, in all but one case, they show similar behaviors to Fig. 1: the trajectories first go from $R = 1$ toward $R = 0$ in an approximately direct path at 1 GHz and then fold into a loop as the frequency is increased to 10 GHz.

III. Dielectric and Magnetic Requirements

In many other fields of technology, it is often possible to know to some order of magnitude whether a particular component is suitable for a design. Consider the simple question as to what value of permeability is suitable for a particular multilayer structure. Suppose, for instance, that it is necessary to do impedance matching for a multilayer medium with a thickness of 3 mm at a frequency of 10 GHz. Suppose that two materials are available with permeability $1-0.1j$ and $3-10j$. Is it obvious which material is suitable and which one is not? Even with computation and optimization, it is not possible to determine the answer with

certainty. In this section, a simple method is discussed that may give an estimate of the suitable permittivity and permeability.

The approach is to examine the quiver plots described in the previous section to determine if there exist any general trend in the directions and magnitudes of the arrows in relation to changes in permittivity and permeability. The vector quantities of the arrows in the unit circle on the complex R plane may be determined by differentiating R with respect to h using (1) and (3) to obtain

$$\left.\frac{dR}{dh}\right|_{h=0} = -\frac{j4\pi}{\lambda(1+Z')^2}(\mu_r - Z'^2\varepsilon_r) \tag{6}$$

where $Z' = Z/K_0$. Equation (6) is derived in the Appendix. Here, $R = R_0$, $Z = Z_1$, and $h = h_1$. We have chosen to omit the subscripts since, in what follows, we shall not be referring directly to the different layers within the mutlilayer structure. This simple formula can be used to quickly compute the arrow directions and magnitudes anywhere in the unit circle. Only a small number of selected points is sufficient, since variations in arrow magnitudes and directions tend to be gradual, as Fig. 3 shows. Equation (6) can be used in a simple way to determine the suitable ranges of permittivity and permeability. Consider first the extreme cases when ε_r and μ_r are large or small. From Fig. 1, since the shortest path from $R = 1$ to 0 is desired, it is likely that in the optimum design the actual path may lie close to the positive real R axis. From (1), the corresponding range of Z' is 0 to 1, i.e., a real number. Using this, (6) can be simplified for the following cases.

Case 1) For large μ_r'' and small μ_r', ε_r', and ε_r''

$$\left.\frac{dR}{dh}\right|_{h=0} \to -\frac{4\pi\mu_r''}{\lambda(1+Z')^2}. \tag{7}$$

Case 2) For large μ_r' and small μ_r'', ε_r', and ε_r''

$$\left.\frac{dR}{dh}\right|_{h=0} \to -\frac{j4\pi\mu_r'}{\lambda(1+Z')^2}. \tag{8}$$

Case 3) For large ε_r' and small μ_r', μ_r'', and $\varepsilon\mu_r''$,

$$\left.\frac{dR}{dh}\right|_{h=0} \to \frac{j4\pi Z'^2\varepsilon_r'}{\lambda(1+Z')^2}. \tag{9}$$

Case 4) For large ε_r'' and small μ_r', μ_r'', and ε_r'

$$\left.\frac{dR}{dh}\right|_{h=0} \to \frac{4\pi Z'^2\varepsilon_r''}{\lambda(1+Z')^2}. \tag{10}$$

The direction of the arrows in the neighborhood of the positive real R axis from 0 to 1 can then be determined for the above cases.

Case 1) For large μ_r'', and small μ_r', ε_r', and ε_r'', the arrow points to the left. See Fig. 3(a).

Case 2) For large μ_r', and small μ_r'', ε_r', and ε_r'', the arrow points downwards. See Fig. 3(b).

Case 3) For large ε_r' and small μ_r', μ_r'' and ε_r'', the arrow points up. See Fig. 3(c).

Case 4) For large ε_r'' and small μ_r', μ_r'' and ε_r', the arrow points to the right. See Fig. 3(d).

These results are illustrated in Fig. 3. In Figs. 3(c) and (d), some arrows along the positive real axis point down because of the finite value of μ_r'. It is interesting that the effects of μ_r'', μ_r', ε_r', and ε_r'' can be so clearly separated. Even though this analysis has only been carried out for the extreme cases, quiver plot visualization shows that the trend remains similar to some extent even for other combinations of values of permittivity and permeability. The above result is immediately useful as a rule of thumb, because it is known from Fig. 1 that the multilayer design may be visualized as the creation of a path going from $R = 1$ to 0. They may also be used to give an estimate of the range of suitable values of permittivity and permeability. First, it is clear that a high magnetic loss material is most desirable, for not only do the arrows in the region between $R = 1$ to 0 point in the desired direction, but the magnitudes of these arrows are also proportional to the magnetic loss, μ_r'', as (7) shows.

To obtain an estimate for the order of magnitude of μ_r'' that is suitable, suppose a medium has a number of layers consisting of a combination of low-loss dielectric and high-loss magnetic materials. Since the effects of μ_r'', μ_r', ε_r', and ε_r'' are clearly separate, each of them can be treated individually. Assume also an ideal case when the trajectory goes from $R = 1$ to 0 and stays close to the real axis, so that it is close to the shortest possible path. We can estimate the total layer thickness of the magnetic layers directly from Fig. 3(a) just by counting the number of arrows. Each arrow (δR) corresponds to a thickness (δh) of 0.1 mm. The word "arrow" here is used in a broader sense than the actual arrow shown in the quiver plot. It is used as a unit of measurement of distance, a unit whose size varies with position on the complex plane. For instance, the size of gaps between the arrows should also be estimated in terms of the number of arrow lengths. Using this idea, we estimate about 12 "arrows" along the real axis, from $R = 1$ to the 20 dB circle. Thus, if a 20-dB reflection is required at 3 GHz, for $\mu_r'' = 10$, this corresponds to a total thickness of magnetic layers of $12\delta h = 1.2$ mm. Conversely, suppose the requirement is for a maximum thickness (H) of 3 mm of magnetic layers. From (5) and (7), since for given $\delta R, \mu_r''$ and δh are inversely proportional, this implies a μ_r'' of $1.2/3 \times 10 = 4$. It should be noted that, even if μ_r'' is different from 4, a design may still be possible if suitable trajectories away from the real R axis can be found, since the above discussion only holds for trajectories close to the real axis.

This, of course, is very approximate, but it nevertheless narrows down the suitable range of permeability from absolutely no knowledge to possibly within an order of magnitude. Returning to the example question in the first paragraph of this section, and assuming that the required multilayer specifications are $H = 3$ mm and $\lambda = 3$ cm, it is now possible to answer more confidently that an average permeability of $1 - 0.1j$ may not be suitable. In fact, if all the available materials were largely dielectric media, then it would be very difficult to design the multilayer structure since, in this case, Fig. 3(c) and (d) shows that there is no direct trajectory movements to the left. (We may, of course, move along the semicircle from $R = 1$ to 0 in Fig. 3(c). This corresponds to a $\lambda/4$ dielectric layer. But then the thickness is greater and it tends to be narrow band.) However, if the available materials have an average μ_r of around $3 - 10j$, then the chance of a successful design is likely to be higher. The thick-

ness of each layer would have to be adjusted to give an average that falls within the suitable range. This may, for instance, be carried out with a combination of the visual design described in the previous section, and optimization.

Turning now to ε_r', it is clear that this cannot be separated from μ_r', since the upward contribution from the former must be designed to compensate for the downward contribution of the latter. Such a relation is clear from Fig. 3(b) and (c). For a given set of magnetic layers and for a particular frequency, it is necessary to select dielectric layers of suitable thicknesses and ε_r' to correct for the "deviation" caused by μ_r'. Note that we have ignored ε_r'' because the dielectric layers are assumed to be low loss in the above discussion.

IV. Design Strategy

Based on the above results, it is possible to design strategies for impedance matching of multilayer structure. First, a few rules of thumb are summarized as follows.

1) Each layer may be represented by a trajectory on the complex R plane.
2) The start of the trajectory corresponds to the surface touching the metal plate, and the end of the trajectory corresponds to the surface in contact with the air.
3) The shape of the trajectory depends on the ε and μ of the layer and is usually curved in the clockwise direction.
4) As the layer thickness increases, the trajectories increase in length.
5) If the material is lossy (i.e., ε_r'' or ε_r'' not zero), all possible trajectories converge to a point given by [16]

$$R = \frac{1 - \sqrt{\mu_r/\varepsilon_r}}{1 + \sqrt{\mu_r/\varepsilon_r}} \tag{11}$$

where ε_r or μ_r are complex.

6) If the material is lossless, the trajectories form closed circles which enclose one another.
7) For the layer touching the metal plate, the trajectory always start from $R = 1 + 0i$.
8) Trajectories of additional layers are cumulative and are joined end to end. That is, the next layer trajectory starts at the end point of the current layer trajectory.
9) The overall amplitude and phase of reflection are given by the end point of the last trajectory.
10) For good impedance matching, this point must be as close to $R = 0$ as possible.

One obvious design strategy is suggested here. Unlike the above rules of thumb which should be true under most conditions, a design strategy may not always work. It may be considered as a method to locate a local optimum. However, a design procedure based on the complex R plane may nevertheless give insight into possible alternatives by giving a more global view of the matching behavior. The following strategy is derived from observation of the behavior of the trajectories in Fig. 2. It assumes that it is better to try to take the straight path from $R = 1$ to $R = 0$ and that a computer is available to generate the required family of trajectories for each material at the frequencies of interest.

1) Along the straight line joining $R = 1$ to $R = 0$, contribution to the trajectory direction is likely to be separable into the following contributions: ε_r' up, ε_r'' right, μ_r' down, and μ_r'' left.
2) The most important contribution therefore comes from μ_r''. If possible, the first layer should have high magnetic loss in order to bring the trajectory as close to $R = 0$ as possible.
3) In real material, the ε_r' or μ_r' may not be small. This would lead to a deviation of the initial trajectory upwards or downwards. It may be possible to compensate for this by using another layer with high ε_r'. The trajectories for such material tend to form small circles on the right half of the R plane as in Fig. 2(b). So the trajectory may be made to move up or down by adjusting its length.
4) The lengths of the first two trajectories should be adjusted until the end point is suitable for the third layer.
5) A high μ_r'' material should again be selected for the third layer, so that there are trajectories traveling left and passing close to $R = 0$. A bundle of such trajectories may be projected backward until they meet the end point of the first two trajectories.

The above strategy assumes essentially three layers: a low-loss dielectric layer sandwiched between two lossy magnetic layers. More layers may of course be added for fine-tuning if materials could be found with trajectories in the right directions. Strategies for other combinations of materials may also be devised. For broad-band matching, the above strategy may be repeated at a few different frequencies within the band of interest. The following additional steps may be considered.

1) Start with the highest frequency. Design the trajectories with a fold in the clockwise direction, as in Fig. 1(c).
2) For lower frequencies, the trajectories will "unwind" in the anticlockwise direction, as in Fig. 1(b). As a result, they will unfold and the end point may move nearer to or further from $R = 0$.
3) If necessary, steps 1) and 2) may then be repeated. Adjusting the lengths of the trajectories can shift the final end point accordingly. The process is repeated until a satisfactory broad-band matching is obtained.

V. Discussion

In this section, we use the ideas from the previous section to design a multilayer structure. Starting with the same design as Fig. 2, which has a dielectric layer sandwiched between two magnetic layers, we vary the thickness of each layer. We monitor the trajectory plots at 1, 3, and 10 GHz, with the intention of getting the final points of the trajectories for all three frequencies into or as close to the inner circle as possible. A MATLAB program has been written for this purpose, with all the trajectories plotted automatically each time a new set of thicknesses is entered. After trial and error for about ten minutes on a computer, the results in Fig. 4 are obtained.

The reflection from this design is compared with the GA results from [10] in Fig. 5. In particular, HF2 has a total thickness of 2.670 mm, which is closest to that in Fig. 4. For only three

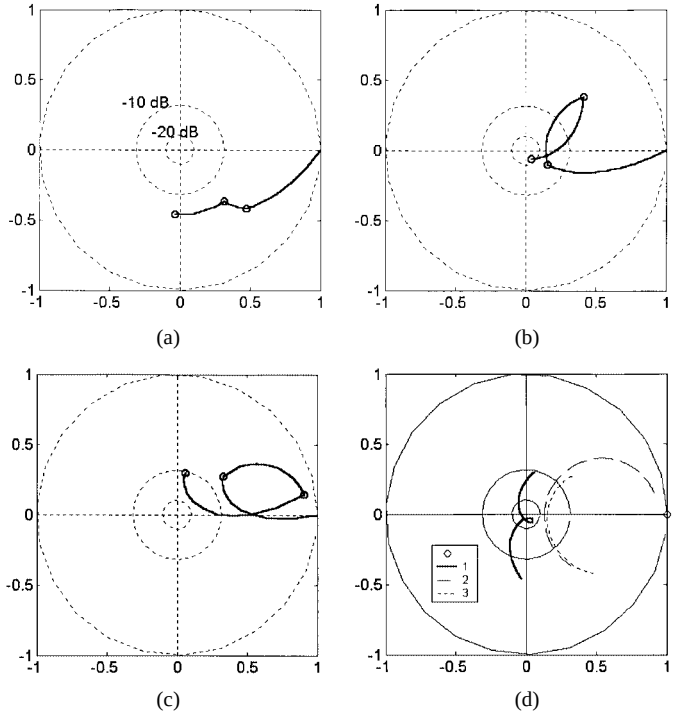

Fig. 4. Trajectory plots of layers 1 to 3, made up of materials number 16, 2, and 13, with thicknesses 0.8, 0.6, and 1.2 mm, at: (a) 1 GHz, (b) 3 GHz, and (c) 10 GHz, respectively. (d) The loci of the endpoints of the trajectory for each layer, from 1 to 10 GHz, is shown.

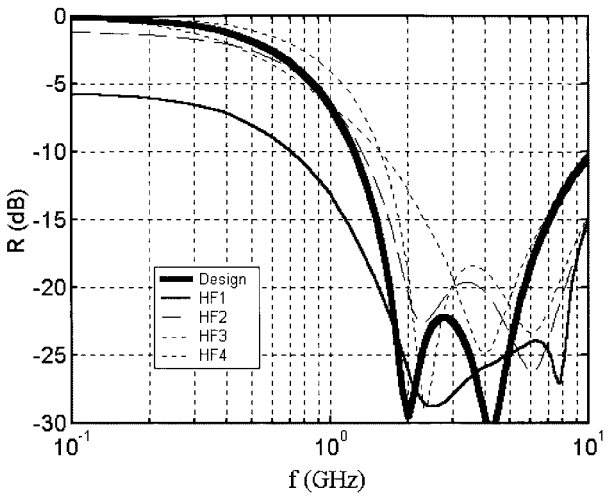

Fig. 5. "Design" is the three-layer structure designed in Fig. 4. HF1-4 are the GA results for five layers each from [10], with total thickness 5.244, 2.670, 1.761, and 1.236 mm, respectively.

layers, it compares favorably with the GA results, which use five layers. It may be argued that our selection of the materials and initial thicknesses have been biased by a prior knowledge of the GA results. However, since the method provides immediate visual information on the variation of R with thicknesses, it should be useful on its own.

In conclusion, we have presented a graphical design method for the multilayer impedance matching problem. It provides a visual picture of each material property and charts out each layer as a curve on a Smith-chart-type figure. This allows an immediate global view of all parts of the problem simultaneously and provides the tools needed for designing intuitively. This method provides greater insight into the problem and can complement existing design methods using optimization techniques.

APPENDIX

In this Appendix, (6) is derived. Suppose that the reflectivity of a multilayer structure is plotted as a point on the complex R plane. When a thin layer of material of thickness is added, the reflectivity may change slightly, and this corresponds to a new point. The objective is to determine this shift on the complex plane. In order to do this, we can make use of (1)–(3). Without loss of generality, we may associate layers 2 to M-1 with the multilayer structure and layer 1 with the thin layer of material. The reflectivity of the multilayer structure is then given by R_0 in (1), with $h_1 = 0$. When the thin layer is added, h_1 is increased to $h_1 + \delta h_1$, and R_0 takes on a new value, $R_0 + \delta R_0$. δh_1 is thus the thickness of this thin layer, and δR_0 is the same as the shift on the complex plane that we want. Using the small increase approximation

$$\delta R_0 \approx \frac{dR_0}{dh_1}\delta h_1 \tag{A1}$$

where the derivative should be evaluated at $h_1 = 0$.

We next obtain a formula for this derivative. Notice from (1) that R_0 depends on Z_1. Z_1 in turn depends on h_1 according to (2). This is reproduced here with $m = 2$ for convenience as follows:

$$Z_1 = K_1 \left[\frac{Z_2 + K_1 \tanh(U_1 h_1)}{K_1 + Z_2 \tanh(U_1 h_1)}\right]. \tag{A2}$$

We shall obtain the derivative using the chain rule

$$\frac{dR_0}{dh_1} = \frac{dR_0}{dZ_1}\frac{dZ_1}{dh_1}. \tag{A3}$$

First we find, from (1)

$$\frac{dR_0}{dZ_1} = -\frac{2K_0}{(K_0 + Z_1)^2}. \tag{A4}$$

Next, from (A2), we have the equation shown at the top of the following page. Evaluating this equation at $h_1 = 0$ gives

$$\left.\frac{dZ_1}{dh_1}\right|_{h_1=0} = \frac{U_1}{K_1}\left(K_1^2 - Z_2^2\right). \tag{A5}$$

Combining (A3), (A4), and (A5) yields

$$\left.\frac{dR_0}{dh_1}\right|_{h_1=0} = -\frac{2K_0}{(K_0 + Z_1)^2}\frac{U_1}{K_1}\left(K_1^2 - Z_2^2\right). \tag{A6}$$

From (A2), when $h_1 = 0$, we have

$$Z_1 = Z_2 \tag{A7}$$

a fact that is also physically obvious since $h_1 = 0$ means that layer 1 is absent. From (3), we have

$$K_1 = \sqrt{\frac{\mu_1}{\varepsilon_1}} \text{ and } U_1 = j\omega\sqrt{\mu_1\varepsilon_1}. \tag{A8}$$

$$\frac{dZ_1}{dh_1} = K_1 \frac{(K_1 + Z_2 \tanh U_1 h_1) K_1 - (Z_2 + K_1 \tanh U_1 h_1) Z_2}{(K_1 + Z_2 \tanh U_1 h_1)^2} (\sec h^2 U_1 h_1) U_1$$

Substituting (A7) and (A8) into (A6) and rearranging yields

$$\left.\frac{dR_0}{dh_1}\right|_{h_1=0} = -\frac{2K_0}{(K_0+Z_2)^2}(j\omega\varepsilon_1)\left(\frac{\mu_1}{\varepsilon_1} - Z_2^2\right). \quad \text{(A9)}$$

Let ε_r and μ_r be the relative pemittivity and permeability, respectively, of layer 1. Then $\varepsilon_1 = \varepsilon_0\varepsilon_r$ and $\mu_1 = \mu_0\mu_r$. Let $Z' = Z_2/K_0$ and notice from (3) that $K_0 = \sqrt{\mu_0/\varepsilon_0}$. Then (A9) becomes

$$\begin{aligned}
\left.\frac{dR_0}{dh_1}\right|_{h_1=0} &= -\frac{2K_0}{(1+Z')^2K_0^2}(j\omega\varepsilon_1)\left(\frac{\mu_1}{\varepsilon_1} - Z_2^2\right) \\
&= -\frac{2K_0}{(1+Z')^2}(j\omega\varepsilon_1)\left(\frac{\mu_1/\varepsilon_1}{K_0^2} - \frac{Z_2^2}{K_0^2}\right) \\
&= -\frac{2K_0}{(1+Z')^2}(j\omega\varepsilon_1)\left(\frac{\mu_1/\varepsilon_1}{\mu_0/\varepsilon_0} - Z'^2\right) \\
&= -\frac{2K_0}{(1+Z')^2}(j\omega\varepsilon_0\varepsilon_r)\left(\frac{\mu_r}{\varepsilon_r} - Z'^2\right) \\
&= -\frac{2\sqrt{\mu_0/\varepsilon_0}}{(1+Z')^2}(j\omega\varepsilon_0)(\mu_r - \varepsilon_r Z'^2) \\
&= -\frac{2}{(1+Z')^2}(j\omega\sqrt{\mu_0\varepsilon_0})(\mu_r - \varepsilon_r Z'^2) \\
&= -\frac{2}{(1+Z')^2}(j\omega/c)(\mu_r - \varepsilon_r Z'^2) \\
&= -\frac{2}{(1+Z')^2}(j2\pi/\lambda)(\mu_r - \varepsilon_r Z'^2) \quad \text{(A10)}
\end{aligned}$$

where we have made use of $c = \omega/k$, $k = 2\pi/\lambda$, and $c = 1/\sqrt{\mu_0\varepsilon_0}$ in the last two steps.

To simplify the notations, we omit the subscripts and let $R = R_0$, $h = h_1$, and $Z = Z_1$ which from (A7) is the same as Z_2 when $h_1 = 0$. This should not cause any confusion since, for (A10), we shall mainly be interested in the distinction between the multilayer structure as a whole and the thin layer that is added on top of it, so that we would not need the subscripts to distinguish between the different layers within the multilayer. Equation (A10) is then the same as (6).

REFERENCES

[1] J. R. Wait, *Electromagnetic Waves in Stratified Media*. New York: IEEE Press, 1995.

[2] J. J. Pesque, D. P. Bouche, and R. Mittra, "Optimization of multilayer antireflection coatings using an optimal control method," *IEEE Trans. Microwave Theory Tech.*, vol. 40, pp. 1789–1796, Sept. 1992.

[3] R. L. Fante and M. T. McCormack, "Reflection properties of the salisbury screen," *IEEE Trans. Antennas Propagat.*, vol. 36, pp. 1443–1454, Oct. 1988.

[4] A. P. Vinogradov, A. N. Lagar'kov, A. K. Sarychev, and I. G. Sterlina, "Multilayer absorbing structures from composite materials," *J. Commun. Technol. Electron.*, vol. 41, pp. 142–145, 1996.

[5] N. L. Dmitruk, O. I. Mayeva, S. V. Mamykin, and O. B. Yastrubchak, "On a control of photon-surface plasmon coupling at a multilayer diffraction grating," in *Proc. 3rd Int. EuroConference on Advanced Semiconductor Devices and Microsystems*, 2000, pp. 445–448.

[6] N. Shida, K. Suga, T. Higuchi, and T. Iida, "Super high density optical disc by using multi-layer structure," in *Optical Data Storage Conf. Dig.*, 2000, pp. 27–29.

[7] C. P. Neo *et al.*, "Smith chart approach to the design of multilayer resistive sheet," *IEEE Microwave Wireless Comp. Lett.*, vol. 13, pp. 24–26, Jan. 2003.

[8] B. Munk, *Frequency Selective Surfaces: Theory and Design*. New York: Wiley, 2000.

[9] C. R. Brewitt-Taylor, P. G. Lederer, F. C. Smith, and S. Haq, "Measurement and prediction of helix-loaded chiral composites," *IEEE Trans. Antennas Propagat.*, vol. 47, pp. 692–700, Apr. 1999.

[10] E. Michielssen, J.-M. Sajer, S. Ranjithan, and R. Mittra, "Design of lightweight, broadband microwave absorbers using genetic algorithms," *IEEE Trans. Microwave Theory Tech.*, vol. 41, pp. 1024–1031, June/July 1993.

[11] D. S. Weile, E. Michielssen, and D. E. Goldberg, "Genetic algorithm design of Pareto optimal broadband microwave absorbers," *IEEE Trans. Electromagn. Compat.*, vol. 38, pp. 518–525, Aug. 1996.

[12] S. Chakravarty, R. Mittra, and N. R. Williams, "On the application of the microgenetic algorithm to the design of broad-band microwave absorbers comprising frequency-selective surfaces embedded in multilayered dielectric media," *IEEE Trans. Microwave Theory Tech.*, vol. 49, pp. 1050–1059, June 2001.

[13] A. R. Foroozesh, A. Cheldavi, and F. Hodjat, "Design of Jaumann absorbers using adaptive genetic algorithm," in *Proc. 5th Int. Antennas, Propagation, and Electromagnetic Theory Symp.*, 2000, pp. 227–230.

[14] B. Chambers and A. Tennant, "Optimized design of Jaumann radar absorbing materials using a genetic algorithm," *Proc. Inst. Elect. Eng.—Radar, Sonar, and Navigation*, vol. 143, pp. 23–30, Feb. 1996.

[15] J. Perini and L. S. Cohen, "Design of broad-band radar-absorbing materials for large angles of incidence," *IEEE Trans. Electromagn. Compat.*, vol. 35, pp. 223–230, May 1993.

[16] J. D. Kraus, *Electromagnetics*. New York: McGraw-Hill, 1992, p. 191.

Kai M. Hock was born in Singapore, in 1966. He received the B.A. (with honors) and Ph.D. degrees in physics from Cambridge University, Cambridge, U.K., in 1988 and 1992, respectively.

From 1992 to 1997, he was with DSO National Laboratories, Singapore, where he was involved with optical engineering and signal processing. From 1997 to 2001, he was a Principal Engineer with the Sony Singapore Research Laboratory, where he was involved with servo control and read/write mechanisms of optical disc systems He is currently a Research Associate Professor with Temasek Laboratories, National University of Singapore, Singapore. His research interest is in microwave materials.